Experimental demonstration of deformable reflector antenna system with high accuracy deformation measurement

Experimental Demonstration of Deformable Reflector Antenna System with High Accuracy Deformation Measurement

Hiroaki Tanaka
National Defense Academy of Japan, Yokosuka, Kanagawa, 239-8686, Japan

Nozomu Kogiso, Fumika Sakano
Osaka Prefecture University, Sakai, Osaka, 599 -8531, Japan

Nobuhisa Katsumata
Kagawa University, Takamatsu, Kagawa, 761 -3496, Japan

Kenji Yamazaki
Honda Motor, Haga, Tochigi Japan

Ken Higuchi, Kosei Ishimura
Waseda University, Tokyo, 169-8555, Japan

Takashi Iwasa
Tottori University, Tottori, Tottori, 680-8550, Japan

Naoko Kishimoto
Setsunan University, Neyagawa, Osaka, 572-8508, Japan

Motoharu Fujigaki
Fukui University, Fukui, Fukui, 910-8507, Japan

Akihiro Doi, Satomi Nakahara, Yutaka Hasegawa
Japan Aerospace Exploration Agency, Sagamihara, Kanagawa, 252-5210, Japan

and
Yusuke Kono
National Astronomical Observatory of Japan, Mitaka, Tokyo, 181-8588, Japan

In this study, an engineering model for a high-precision reflector antenna system equipped with a deformable sub-reflector with six actuators and a two-dimensional (2D) grating measurement system was developed. In this system, a deformation of the main reflector of the antenna system was measured by a 2D grating measurement system. Then, the path length error due to the deformation was compensated by adjusting the shape of the deformable sub-reflector. Novel path length error correction procedure for obtaining shape control inputs from shape measurement results was also developed. In this method, the antenna deformations of the entire reflector area were estimated from the measured deformations at

few points to decrease the measurement durations. An experiment was carried out to investigate the effectiveness of the developed system and the limitation of the deformable reflector with small number of actuators. In the experiment, the main reflector was intentionally deformed by applying a load, and the resultant path length error was compensated by using the deformable sub-reflector system. The changes in the power of radio waves received from a satellite were measured during the experiments, and the effectiveness of the developed system was investigated. The deteriorated reception power due to the deformation of the main reflector was recovered to some extent by adjusting the shape of the deformable reflector. Thus, the findings demonstrated the effectiveness of the developed smart reflector antenna system and also indicated the limitation caused by the difference between the deformation shapes of the main reflector and the deformable reflector.

Keywords

Deformable reflector, High accuracy deformation measurement, Path length error control, Piezoelectric actuator, Space antenna, Smart structure,

Nomenclature

$\boldsymbol{a}$ = optimally allocated actuator outputs

a_{limit} = stroke limit of actuators

$\boldsymbol{a_z}$ = coefficients of Zernike modes

$\boldsymbol{d}$ = deformations at the evaluation points on the main reflector

$\boldsymbol{d_m}$ = measured deformations on the reflector

$\boldsymbol{M_z}$ = matrix indicating the amplitudes of each Zernike mode at the evaluation points

$\boldsymbol{M_{zm}}$ = matrix indicating the amplitudes of each Zernike mode at the measurement points

N_e = number of evaluation points

P_0 = reception power at the nominal pointing direction

P_{az+} = reception power in the direction where the azimuth angle was changed from nominal by $+\theta_{az}$

P_{az-} = reception power in the direction where the azimuth angle was changed from nominal by $-\theta_{az}$

P_{el+} = reception power in the direction where the azimuth angle was changed from nominal by $+\theta_{el}$

P_{el-} = reception power in the direction where the azimuth angle was changed from nominal by $-\theta_{el}$

P_{sky} = background reception power

$\tilde{P}_{*}$ = reception power in which the effect of the background power was eliminated

$Z(1, -1)$ = vertical tilt mode

$Z(1, 1)$ = horizontal tilt mode

$Z(2, 0)$ = defocus mode

$Z(2, 2)$ = vertical astigmatism mode

Z_{ref} = distance between two reference surfaces

α_i = weighting factor calculated based on the areas where the point is representative and radio field intensity

ΔZ = relative deformations of the main reflector

$\Delta\varepsilon_i^{main}$ = half-path length error due to the deformation of the main reflector at the *i*-th evaluation point

$\Delta\varepsilon_i^{sub}(\boldsymbol{a})$ = half-path length error due to the actuation of the deformable sub-reflector at the *i*-th evaluation point

$\Delta\Phi$ = change in phase of grating on the same pixel between the images of reference surface 1 and the deformed surface

$\Delta\Phi_{ref}$ = change in phase of grating on the same pixel between the captured images of the two references

θ_{az} = movement of the antenna direction from the nominal pointing direction in the azimuth angle

θ_{el} = movement of the antenna direction from the nominal pointing direction in the elevation angle

Θ = boundary-layer momentum thickness

ρ = density

Subscripts

cg = center of gravity

G = generator body

iso = waypoint index

1. Introduction

Large and accurate reflector space antennas are needed to achieve high-performance missions, such as observing celestial objects in extremely high-frequency bands (30–300 GHz) or 5G satellite communication. Large reflector space antennas are required to be lightweight and deployable, and they are easily deformed owing to disturbances. To realize high-accuracy optics of large reflector systems, deformable reflector systems have been investigated [1–12]. In these systems, path length errors due to the deformations of the main reflector are compensated by adjusting the shape of the deformable reflector. The concept of the path length error compensation is same as wavefront control for optical reflector. However, a completely different system is required for a radio wave antenna owing to differences in wavelength. For example, several orders larger shape changes are required in deformable reflector.

Fang et al. developed a 2.4-m engineering model equipped with 84 polyvinylidene difluoride (PVDF) actuators and investigated the adaptive surface control of the membrane reflector [2]. Several experimental studies have been conducted that demonstrate the feasibility of the membrane reflector for high precision adaptive control architecture. Datashvili et al. developed laboratory models of reconfigurable reflectors that employed a carbon fiber-reinforced silicon (CFRS) surface and studied their reconfiguration possibilities [3]. This reflector had 91 actuators that helped achieve an object surface shape. Bradford et al. developed an active composite reflector panel equipped with 90 macro-fiber composite (MFC) actuators to correct wavefront errors in the reflector and demonstrated its feasibility [4]. In the study, thermally-induced surface deformations were deliberately introduced into the reflector and corrected to a tolerance of 50 nm using the actuators. Wang et al. developed the novel shape adjustment method for cable net structures with lead zirconate titanate (PZT) actuators [5]. The PZT actuators were incorporated in active cables and used for shape adjustment. The feasibility of the system was demonstrated through numerical simulations. Xie et al. investigated the feedback shape control method for deployable mesh reflectors using the gain scheduling method, and the method was applied to compensate thermal deformations [6]. The effectiveness of the method was demonstrated through numerical simulations. JiaFu et al. proposed the surface shape control method of a reflector by actively modulating the solar radiation pressure force using reflectivity control devices [7]. The surface shape of slack reflector with negligible elastic deformations was controlled to be a paraboloid using the proposed method. Molaei et al. developed the origami inspired reconfigurable antenna system [8]. This antenna system can change its operational frequency, direction of maximum radiation pattern, and maximum realized gain by using origami structure, which can change its shape. The electrostatically forming reflector systems are good candidates for achieving a high accuracy

reflector system [9], and many studies were carried out on the electrostatically forming reflector systems. In the electrostatically forming reflector systems, the shape of the reflector can be controlled using electrostatic forces. Zhang et al. developed the electrode grouping optimization approach for an electrostatic forming membrane reflector antenna [10]. This method is useful to reduce the required weight, power, and costs to maintain certain shape control abilities. Chao et al. proposed a comprehensive structural optimization method for electrostatic forming membrane reflector antennas [11]. This study developed the coupled electrical-structural field analysis mode and applied it for design optimization. Gu et al. developed another type of coupled electrostatic structural field model in electrostatically controlled membrane reflector antennas [12]. A two-meter curved antenna model was developed and the effectiveness of the method was investigated. However, these studies mainly focused on the structural aspect of the deformable reflector system and paid less attention to the performance of the antenna system, and only a few studies investigate the performance of the actual reflector system with a deformable reflector. For the usage of a deformable reflector system in a practical mission, a measurement system for the deformations or path length errors of a reflector is required. However, a practical deformation measurement system used in orbit has not been considered in previous studies.

The authors also developed a prototype of a deformable reflector system, as shown in Fig. 1 [1], and the schematic of the prototype is illustrated in Fig. 2. The deformable reflector was designed as a sub-reflector of a space antenna and was used to compensate for the path length errors in the reflector antenna system. Figure 3 shows a concept of the antenna system equipped with the deformable sub-reflector. The deformable reflector consisted of a solid surface, supporting the column, base plate, and six surface adjustment actuators. The surface adjustment actuator consisted of a piezoelectric stack actuator (PSt 150/10/100 VS15; Piezomechanik GmbH) and a displacement magnification mechanism developed in-house. The displacement magnification mechanism was actuated by the piezoelectric stack actuator, and it magnified the input displacement by approximately 10 times. The actuators have strokes of more than 1 mm with an accuracy of 0.01 mm. The topology of the deformable reflector surface was investigated [13], and the solid surface was designed to have six petals to enlarge the achievable deformation application to radio wave antenna. A surface adjustment actuator was placed behind each petal on its center line to avoid twist deformation of the petal. The surface adjustment actuators pushed the petals from the rear of the solid surface toward the horn antenna, and each petal could be bent like a cantilever beam. The positions of the surface adjustment actuators are shown in Fig. 4. Compared with the deformable reflectors developed in the previous studies [2-4, 12] that have many actuators and amplifiers, this deformable reflector was simple and could be equipped on small sized satellite systems.

The prototype was installed on the reflector antenna system as a sub-reflector, and its effectiveness was experimentally demonstrated. The antenna's main reflector was used as a demonstrator for a balloon -borne very long baseline interferometry (VLBI) mission [14]. Accordingly, the surface of the antenna main reflector was manufactured to be an ideal parabola, whereas the surface modifications of the deformable sub-reflector acted as surface errors to the antenna optics. In the experiments, the changes in the power of the received radio waves were evaluated, and the shapes of the deformable sub-reflector changed. The performance of the deformable reflector system was demonstrated through experiments. However, the feasibility of compensating the path length errors due to the surface deformations of the main reflector by adjusting the shape of the deformable sub-reflector was not demonstrated. Furthermore, our previous study did not take into account that a practical deformation measurement system used in orbit was not previously considered.

Many systems for deformation measurements have been investigated. Photogrammetric systems are often used for the shape measurement of a reflector antenna on the ground [15]. In these systems, many pictures are required to obtain an accurate reflector shape. Therefore, the movement mechanism of a camera or the usage of many cameras are necessary, which makes the use of photogrammetric systems in orbits difficult. Radio haplography is a powerful tool for diagnosing the path length errors of a reflector system [16]. However, it requires appropriate radio wave sources, which are difficult to find in orbits. Some studies developed the shape reconstruction methods of flexible structures using distributed multipurpose sensors [17,18]. These methods can simplify the system using the same sensors for multiple purpose, but the measurement accuracies of such methods are insufficient for the development of high accuracy antenna systems. Grating projection methods can measure the shape or deformation of an object without contact using one or two cameras [19, 20]. Because measured data are provided on a pixel-to-pixel basis, the grating projection method can capture the object surface shape with high spatial resolution and can measure the slight disturbance of the reflector surface shape from the designed value in detail. Therefore, they are good candidates for measuring the deformations of space antennas. A grating pattern is projected on an object, and changes in the phases of the pattern between non-deformed and deformed objects are analyzed to measure the deformation of the object [19]. A grating projection method has also been investigated using pasted grating patterns [20]. In the developed measurement system, a two-dimensional (2D) grating is pasted on a reflector surface instead of the projection, and the deformation of the reflector was measured using the sampling moiré method. This method requires neither a projector nor reference planes, whereas the conventional grating projection method requires reference planes and projection of

the grating from a projector. The calibration of the measurement system is directly conducted using the reflector surface with a pasted grating pattern. Thus, the developed method has the potential to conduct the calibration of the measurement system during the operation in orbits, which provides high-precision measured data without affecting the variation of the surrounding environment. In addition, because the developed measurement system applies a single digital camera to measure the displacement of the reflector surface, the installation restriction of the digital camera that will be a matter in the design process of the traditional satellite is significantly relaxed. However, its applicability to a high-precision deformable reflector antenna has not been demonstrated. The ability to measure the deformation of the entire region is useful for diagnosis of the reflector; however, it is time consuming and difficult to control orbit shape.

Therefore, in this study, an engineering model for a high-precision reflector antenna system equipped with a deformable sub-reflector with small number of actuators and a 2D grating measurement system was developed. Furthermore, a novel path length error correction procedure for obtaining shape control inputs from limited shape measurement results was also developed. In this method, the antenna deformations of the entire reflector area were estimated from the measured deformations at a small number of measurement points to decrease the measurement durations. This high-precision reflector antenna concept will be employed in the balloon-borne VLBI mission [14], in which the antenna system will be operated in the stratosphere. To demonstrate the effectiveness of the developed antenna system and the path length error correction procedure and the limitation of the deformable reflector with small number of actuators, an experimental demonstration was conducted. In the experiment, the main reflector of the antenna system was deformed by applying a load, and the deformation was measured by a 2D grating measurement system. Then, the path length error due to the deformation was compensated by adjusting the shape of the deformable sub-reflector. The adjusting quantity as output deformations of the embedded actuators was obtained by applying the optimization method. The changes in the power of radio waves received from a satellite were measured during the experiments, and the effectiveness and the limitation of the developed reflector system was investigated.

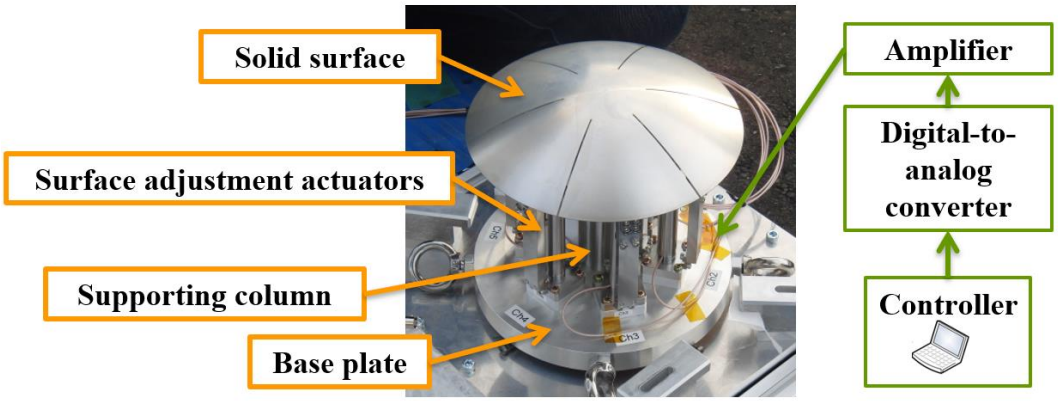

Fig. 1 Prototype of the deformable reflector [1].

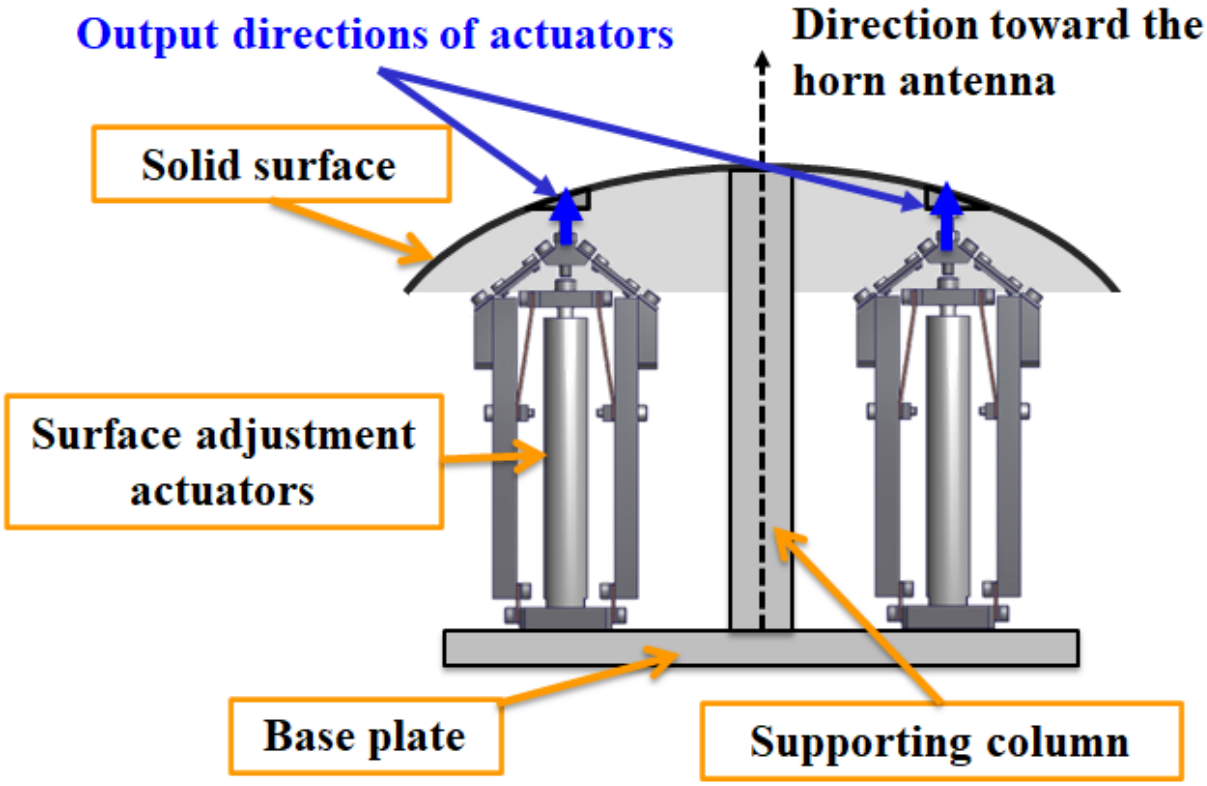

Fig. 2 Schematic of the deformable reflector.

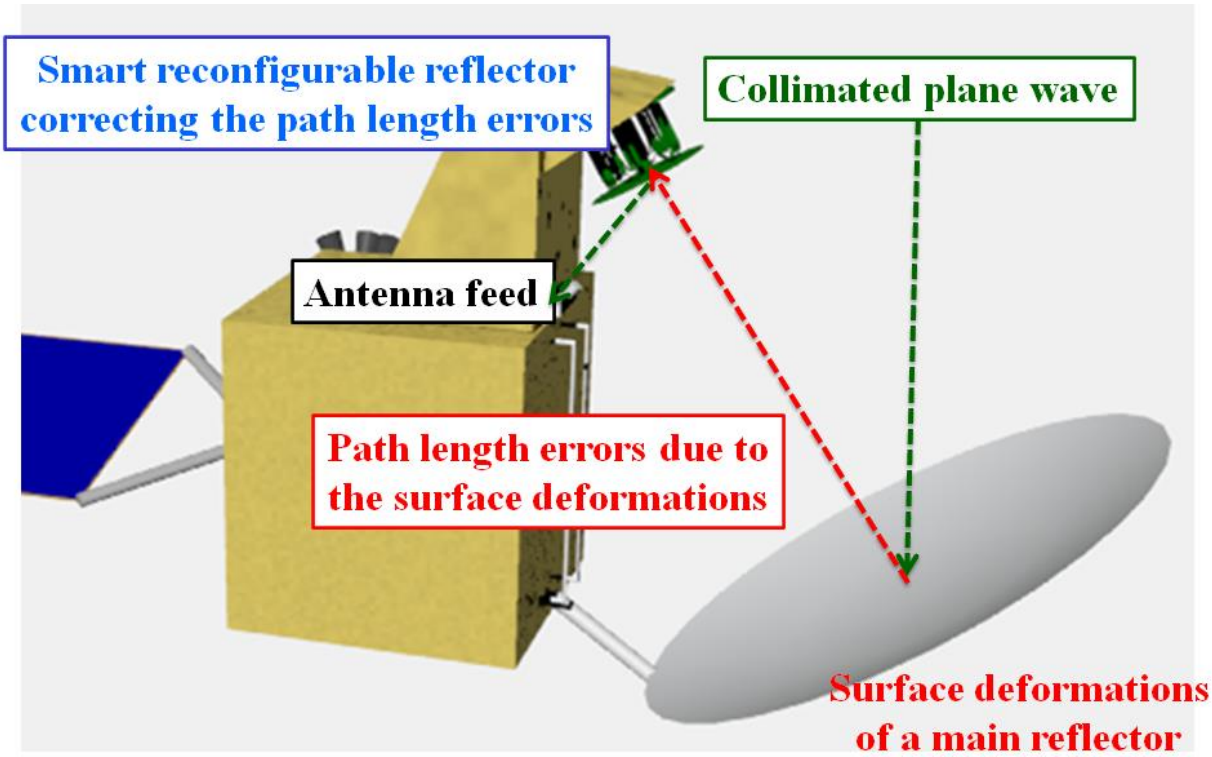

Fig. 3 Schematic of the high accuracy antenna system equipped with the deformable sub-reflector [1].

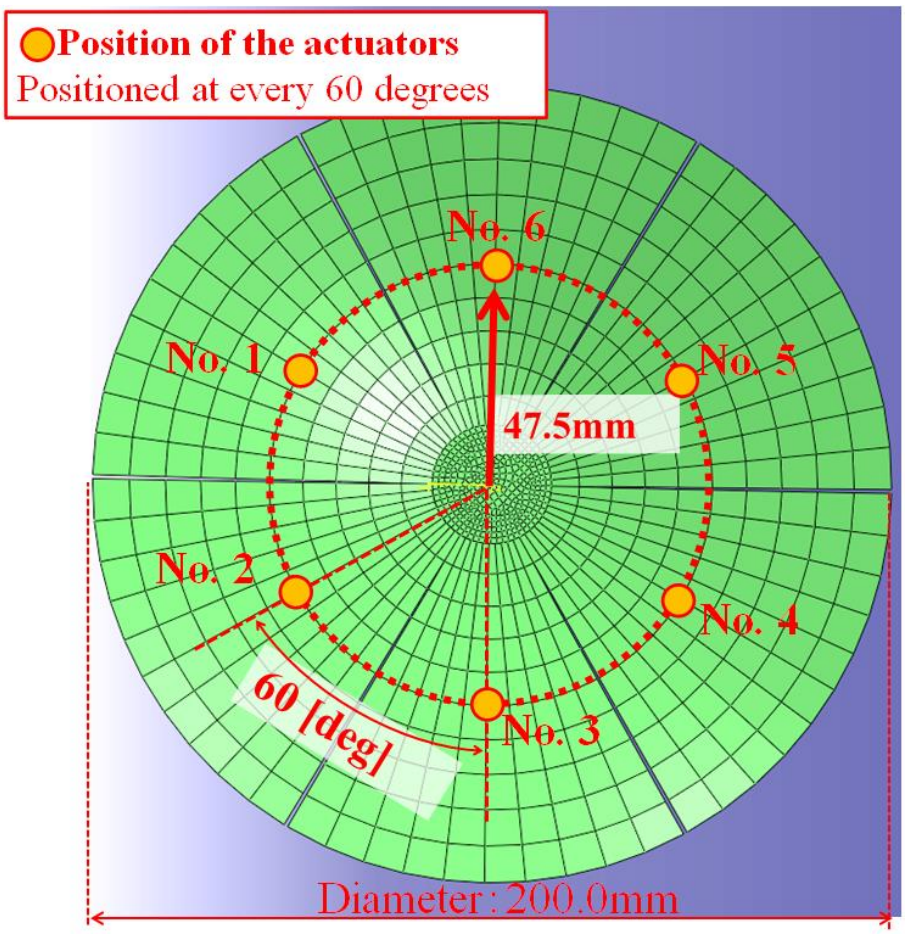

Fig. 4 Position of surface adjustment actuators.

2. High-Precision Reflector Antenna System Equipped with a Deformable Sub-Reflector and 2D Grating Measurement System

2.1 Outline of the Reflector Antenna System

To achieve a high-accuracy optical system, a reflector antenna system equipped with a deformable sub-reflector and a 2D grating measurement system was developed. Hereafter, we call this antenna system as a "smart reflector system." Figure 5 shows the developed smart reflector system. Only one of the two cameras shown in Fig. 5 was used for the deformation measurements. The smart reflector system is a Cassegrain reflector system that consists of a main reflector, a deformable sub-reflector, and the deformation measurement system using a 2D grating method. The 2D grating patterns were pasted on the main reflector and are used for the deformation measurement. The smart reflector system also has a horn antenna, and the antenna can receive actual radio waves from a communication satellite. The diameter and focal length of the main reflector are 1.5 m and 488 mm, respectively. The deformable sub-reflector

system developed in our previous study, as shown in Fig. 1, was employed as the sub-reflector of the antenna system. Fig. 6 shows the geometric relationships of the reflector system. The specifications of the deformable sub-reflector are summarized in Table 1. In the system, the deformation of the main reflector was measured by the 2D grating measurement system, and the path length error due to the deformation of the main reflector was compensated by adjusting the shape of the deformable sub-reflector. The path length errors of the reflector system caused by the deformation and shape control of the deformable sub-reflector were analyzed using a geometrical optics analysis method; an example of ray path is shown in Fig. 6.

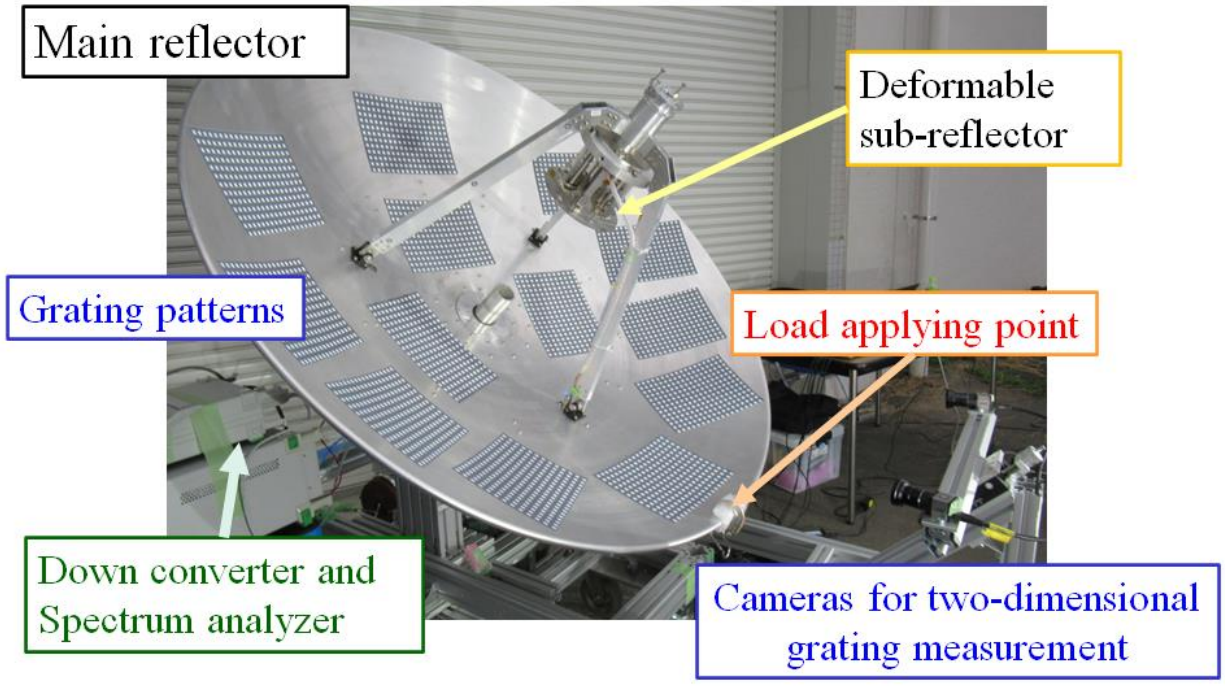

Fig. 5 Photograph of the developed smart reflector system.

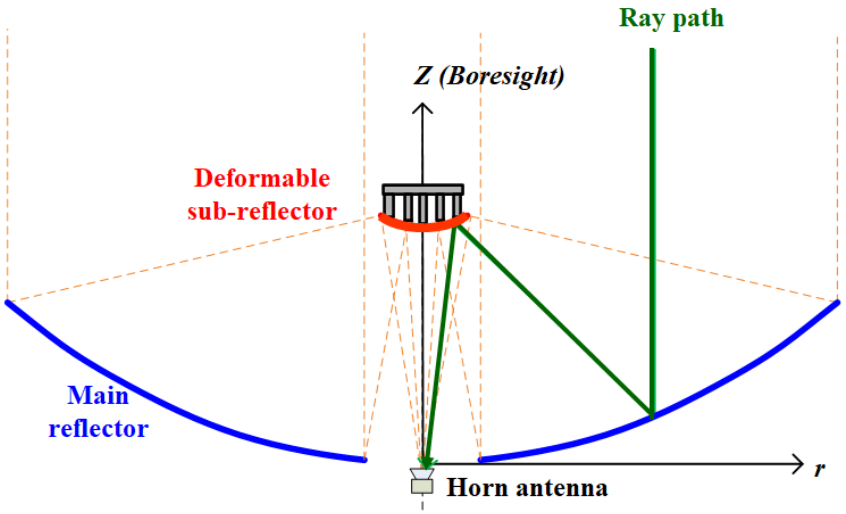

Fig. 6 Geometric relationships of the reflector system.

Table 1 Specifications of the deformable sub-reflector

Category	Specifications
Solid surface	Hyperbolic aluminum reflector with 6 slits: diameter = 200 mm, thickness = 0.5 mm
Surface adjustment actuator	Piezoelectric actuator (PSt 150/10/100 VS15; Piezomechanik GmbH) and displacement magnification mechanism: stroke = approximately 1 mm, number of actuators = 6
Amplifier	Input = 0–10 V, output = 0–150 V

2.2 Deformation Measurement System

A 2D grating with a single camera method was developed based on the sampling moiré method [19]. The 2D grating patterns were pasted on the reflector, as shown in Fig. 5. The grating pattern used in this experiment is shown in Fig. 7. The two images of the grating patterns on the non-deformed reflector surfaces were captured in advance while changing the reflector position. The camera position was changed instead of changing the reflector position in this experiment. The two images were used as the two references, and a three-dimensional coordinate system was created between the two reference surfaces. The geometric relationships of these surfaces are shown in Fig. 8. Then, the image of the pattern on the deformed reflector was captured, and the changes in the pattern phase at any pixel were analyzed to obtain the relative deformations. Fig. 9 illustrates the relation between the relative deformations of the reflector, ΔZ, and the pattern phase obtained from the phase analysis of the 2D grating pattern. From the figure, the relative deformations ΔZ at any pixel were obtained as follows:

$$\Delta Z = \frac{\Delta \Phi}{\Delta \Phi_{ref}} Z_{ref} \qquad (1)$$

Here, Z_{ref} is the distance between the two reference surfaces, $\Delta \Phi_{ref}$ is the change in phase of grating on the same pixel between the captured images of the two references, and $\Delta \Phi$ is the difference in phase of grating between the images of the reference surface 1 and the deformed surface. Deformations at every pixel on the pasted grating patterns can be obtained by this method. However, such a process takes a long time. Therefore, the deformations at the center points of the seven areas shown in Fig. 10 were used for the shape control of the deformable reflector to save time in the experiment.

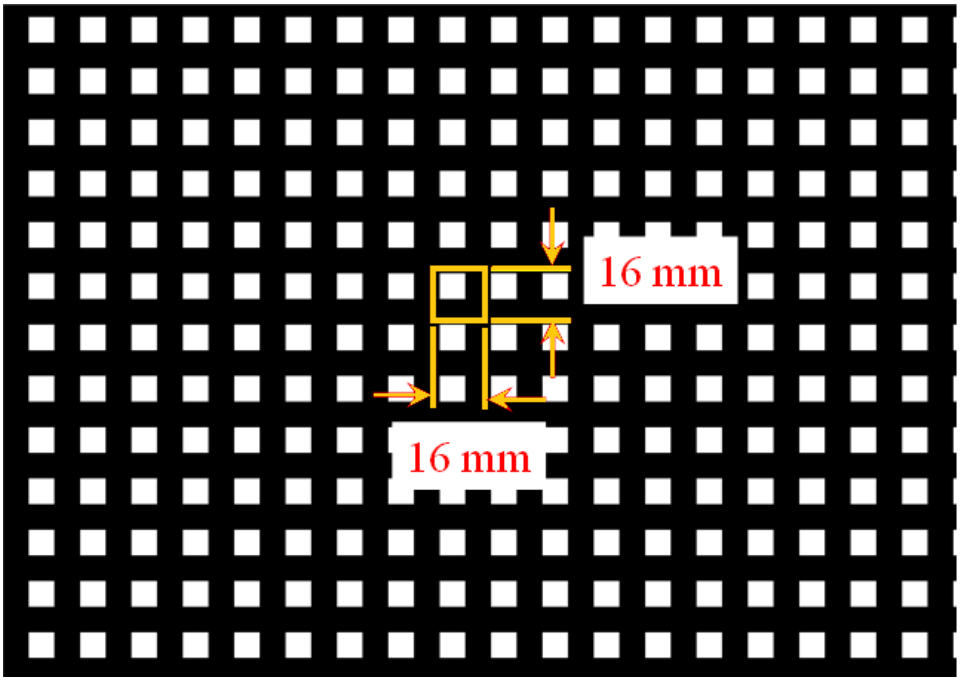

Fig. 7 Pasted grating pattern used in this experiment.

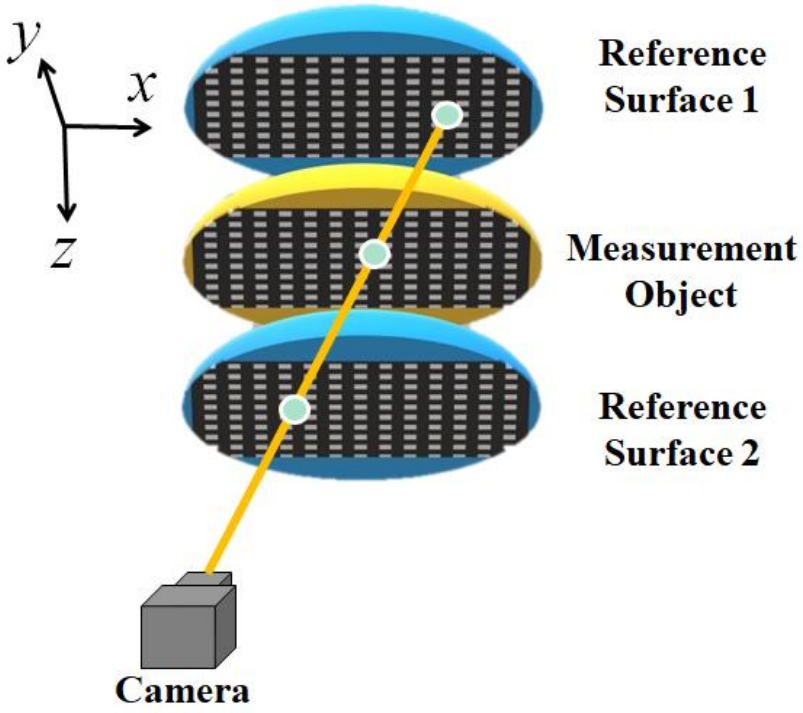

Fig. 8 Geometric relationships of surfaces in the 2D grating and single-camera method.

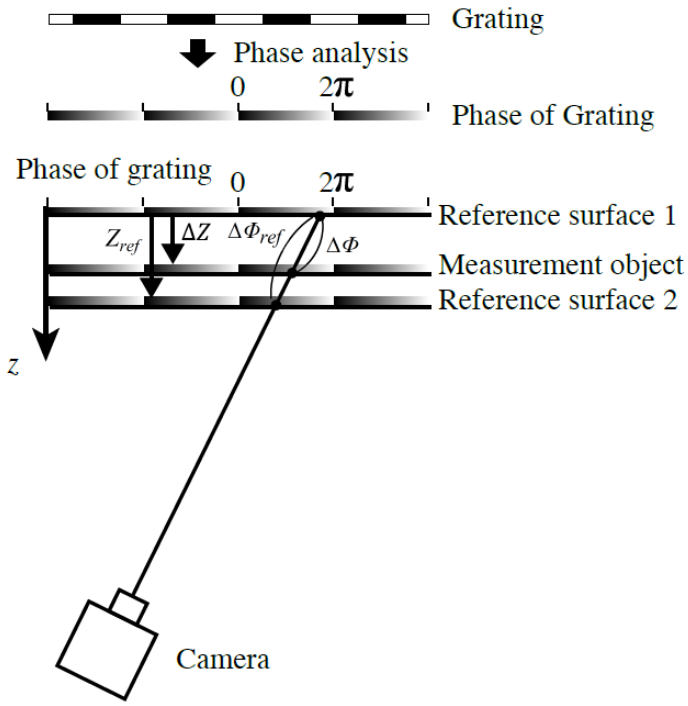

Fig. 9 Relation between relative deformation and pattern phase.

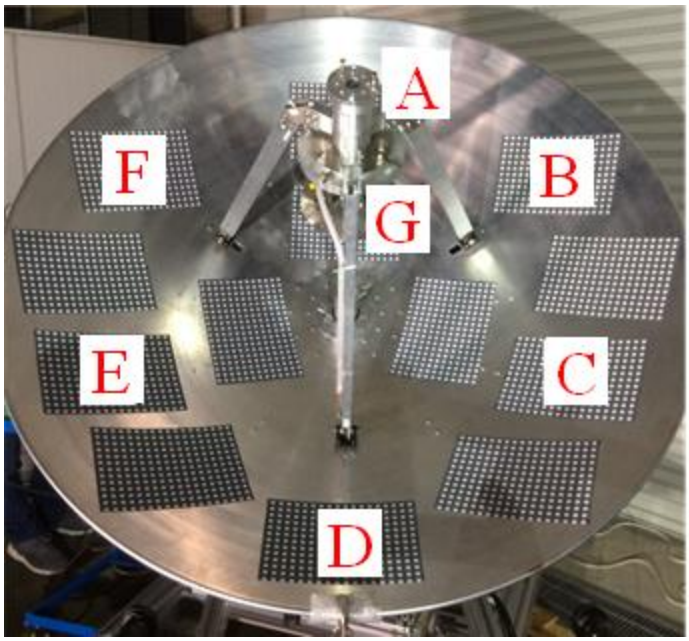

Fig. 10 Deformation measurement points.

2.3 Path Length Error Correction Procedures

A path length error correction procedure to obtain shape control inputs from shape measurement results is developed. The 2D grating measurement system is able to measure deformations at millions of points. However, the measurements at these million points are time consuming that take approximately 30 minutes using laptop PC (Core i7-5500U, Memory 8GB). It may take several hours using an onboard computer on a satellite, which is not suitable for shape control on orbit. Therefore, in this procedure, deformations at the small number of measurement points on the reflector are used to achieve the path length error compensation in a limited time, and a deformation estimation process was included. In the process, Zernike polynomials are employed to estimate the deformations of the whole reflector from the limited deformation measurement results. Subsequently, the shape control inputs are obtained using the optimization method. Duration for the shape measurement was reduced to a few minutes using this process. The following points describe the details of the procedure.

The effects of the actuations of the deformable sub-reflector on the path length errors of the antenna optics at the evaluation points, were analyzed through finite element analysis and a geometrical optics analysis beforehand. Fig. 11 shows the finite element model of the deformable sub-reflector. Furthermore, the antenna deformations of the entire reflector area were estimated from the measured deformations at a small number of measurement points. In this experiment, the deformations at the seven points shown in Fig. 10 were measured before and after hanging a weight

at the load application point as shown in Fig. 5. Zernike polynomials were utilized to estimate the deformations of the entire reflector area from the measured deformation data. Zernike polynomials are suitable for expressing the deformation of the circular aperture reflector and are used for reflector analyses in some studies [21, 22]. The coefficients of Zernike modes, $\boldsymbol{a_z}$, were obtained from the deformations measured by Zernike decomposition.

$$\boldsymbol{a_z} = \boldsymbol{M_{zm}^{-}}\boldsymbol{d_m} \qquad (2)$$

Then, the deformations at the evaluation points on the main reflector, $\boldsymbol{d}$, were calculated as the summation of the Zernike modes as follows:

$$\boldsymbol{d} = \boldsymbol{M_z}\boldsymbol{a_z} = \boldsymbol{M_z}\boldsymbol{M_{zm}^{-}}\boldsymbol{d_m} \qquad (3)$$

Here, $\boldsymbol{d_m}$ denotes the measured deformations at measurement points on the reflector, and the deformation on each measurement point was obtained from equation (1). $\boldsymbol{M_z}$ and $\boldsymbol{M_{zm}}$ are the matrices indicating the amplitudes of each Zernike mode at the evaluation points and measurement points, respectively; and $\boldsymbol{M_{zm}^{-}}$ is the pseudo inverse of matrix $\boldsymbol{M_{zm}}$. The dominant deformation modes of the main reflector were investigated using a photogrammetric system before the experiment, and the results revealed that that the tip, tilt, and vertical astigmatism mode were dominant and accounted for 98% of the deformation. Therefore, four Zernike modes, i.e., tip, tilt, defocus, and vertical astigmatism, were employed for the decomposition.

The half-path length error due to the deformation of the main reflector at the *i*-th evaluation point was obtained by a geometrical optics analysis. Then, the actuator outputs of the deformable sub-reflector were determined to minimize the path length error due to the deformation of the main reflector. The optimization problem was formulated to obtain the optimally allocated actuator outputs, $\boldsymbol{a}$, as follows:

$$\text{Minimize}: \ f(\boldsymbol{a}) = \left[\frac{1}{N_e}\sum_{i=1}^{N_e} \alpha_i \left(\Delta\varepsilon_i^{main} - \Delta\varepsilon_i^{sub}(\boldsymbol{a})\right)^2\right]^{\frac{1}{2}} \qquad (4)$$

$$\text{subject to: } 0 \le a_j \le a_{limit}$$

Here, $\Delta\varepsilon_i^{main}$ is the half-path length error due to the deformation of the main reflector at the *i*-th evaluation point, $\Delta\varepsilon_i^{sub}(\boldsymbol{a})$ is the half-path length error due to the actuation of the deformable sub-reflector at the *i*-th evaluation point, a_{limit} is the stroke limit of the actuators, N_e is the number of evaluation points, and α_i is the weighting factor calculated based on the areas where the point is representative and radio field intensity. The limited-memory Broyden–Fletcher–Goldfarb–Shanno with boundaries (L-BFGS-B) algorithm, a quasi-Newton method [23], was used to obtain the optimum outputs. In the deformable sub-reflector, six surface adjustment actuators were installed and numbered, as

shown in Fig. 12. In this study, piezoelectric actuators were used as the surface adjustment actuators, and only the extension of the actuators was available. The stroke limit of the actuator was 1 mm. Therefore, an extension of 0.5 mm was set as the nominal state.

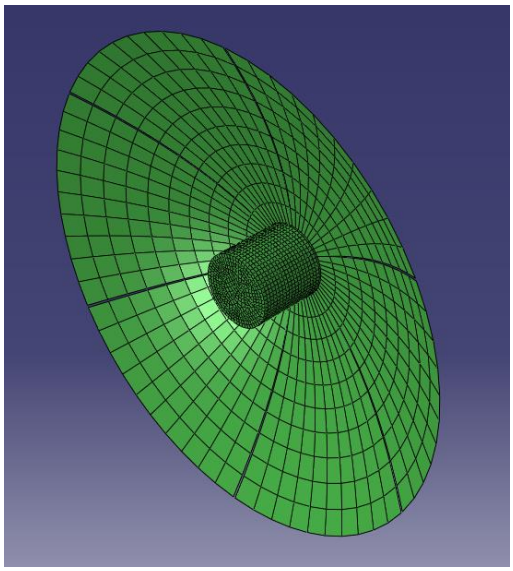

Fig. 11 Finite analysis model of the deformable sub-reflector.

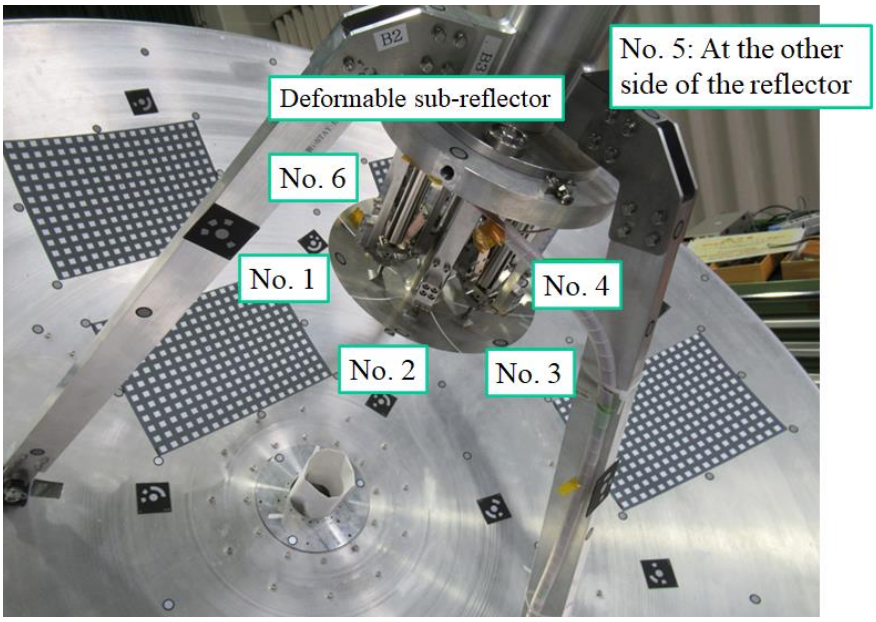

Fig. 12 Numbering of the actuators of the deformable sub-reflector.

3. Experiments

3.1 Experimental Setup

To demonstrate the effectiveness of the developed smart reflector system, an experiment was performed. A schematic representation of the experimental setup for the performance evaluation is illustrated in Fig. 13. In the experiment, a weight of 4.5 kg was applied to the load application point, as shown in Fig. 14, resulting in an external load of 44.1 N being applied to the main reflector. A counterweight was also applied to the antenna system to balance the moment around the elevation axis. The counterweight did not deform the main reflector because it was applied to the shaft. The elevation angle of the reflector system was set to 41.5° so as to receive radio waves from IPSTAR, a communications satellite of Thaicom Public Company Limited. The deformation due to the external load was measured using the 2D grating measurement system. Then, the path length error due to the deformation was compensated by the deformable sub-reflector through the procedure explained in the previous section. Radio waves from IPSTAR were received by the antenna during the experiment, and their power was measured at each experimental step. The frequency of the radio waves was approximately 20 GHz. The received radio waves were down-converted to the 1 GHz range by a down-converter developed in-house to meet the range requirement for sensors used in this study. The down-converted radio waves were analyzed using a spectrum analyzer. To estimate the peak reception power of the radio waves, a "five-point method" was used for each power measurement [24]. In the five-point method, the reception power at the nominal pointing direction, P_0, was measured. Then, the azimuth or elevation angles were changed from the nominal angle by $\pm\theta_{az}$ or $\pm\theta_{el}$, respectively, and changes in the reception power were measured. The background level was also measured by pointing the antenna to a point far from the satellite. The reception power of these measurements was P_{az+}, P_{az-} P_{el+} P_{el-}, and P_{sky}. An example of the reception power during the measurement for the five-point method is shown in Fig. 15. The sampling rate of the power measurement was 10 Hz. An average of 120 measured powers was used as the reception power for each step, and they are plotted as red circles in Fig. 15. For any general power measurement, P_*, the effect of the background level was eliminated as follows:

$$\tilde{P}_* = 10 \times \log_{10}\left(10^{P_*/10} - 10^{P_{sky}/10}\right) \qquad (5)$$

Then, the peak reception power of the radio waves and the angles from the nominal pointing direction were estimated by the following equations:

$$\tilde{P}(\theta_{az}, \theta_{el}) = a\,\theta_{az}^2 + b\,\theta_{az} + c\,\theta_{el}^2 + d\,\theta_{el} + \tilde{P}_0 \qquad (6)$$

$$\theta_{az} = -b/2a \qquad (7)$$

$$\theta_{el} = -d/2c \qquad (8)$$

Here, the coefficients are calculated as follows:

$$a = \left(\tilde{P}_{az+} + \tilde{P}_{az-} - 2\,\tilde{P}_0\right)/\,2\,/\theta_{az}^2 \qquad (9)$$

$$b = \left(\tilde{P}_{az+} - \tilde{P}_{az-}\right)/\,2\,/\theta_{az} \qquad (10)$$

$$c = \left(\tilde{P}_{el+} + \tilde{P}_{el-} - 2\,\tilde{P}_0\right)/\,2\,/\theta_{el}^2 \qquad (11)$$

$$d = \left(\tilde{P}_{el+} - \tilde{P}_{el-}\right)/\,2\,/\theta_{el} \qquad (12)$$

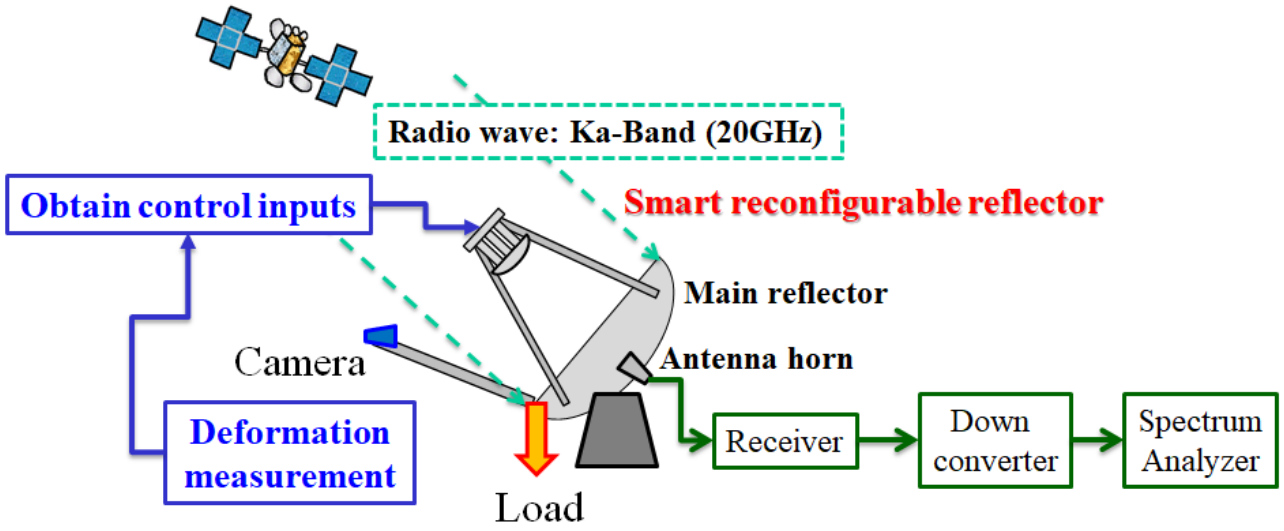

Fig. 13 Overview of the experimental setup.

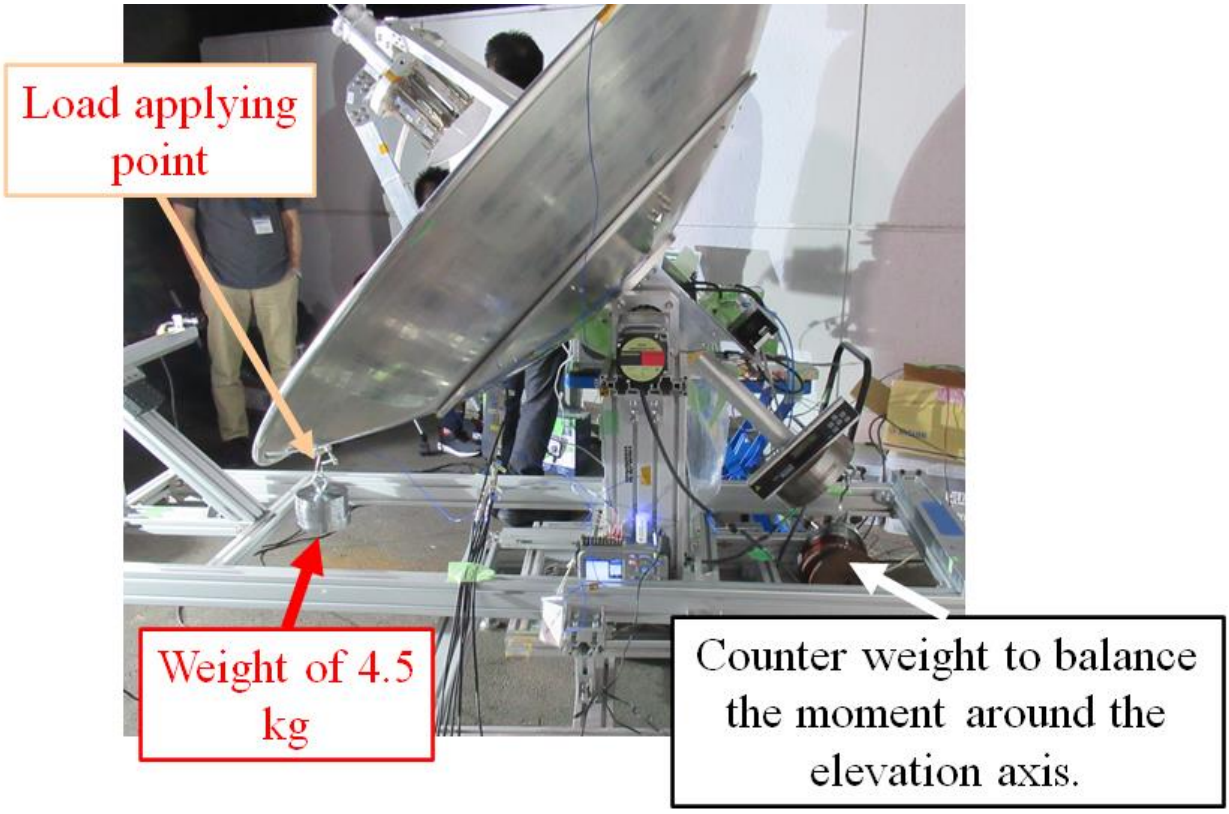

Fig. 14 Applied weight on the reflector and the counter weight.

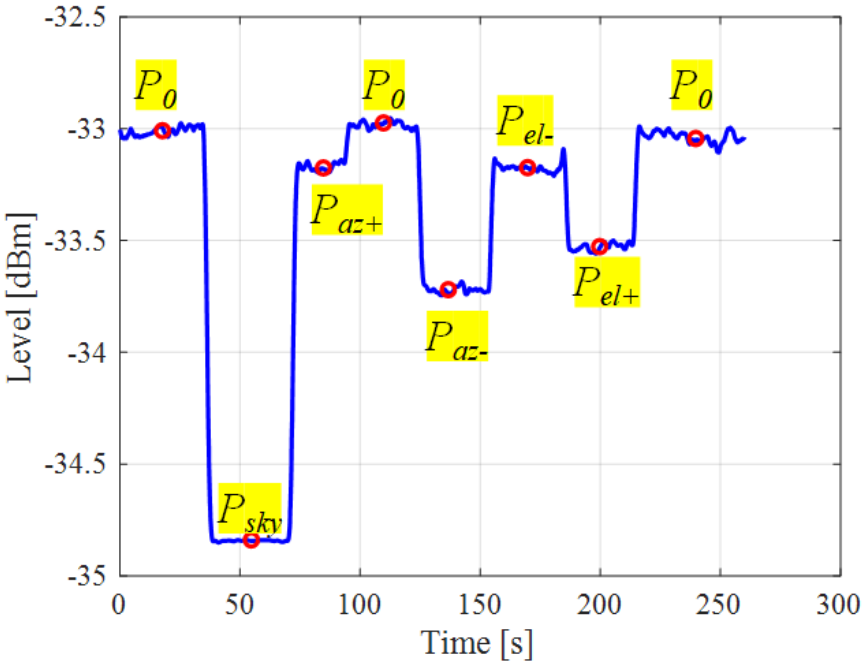

Fig. 15 Example of the reception power for the five-point method.

3.2 Results of the Experiments

The experiments were performed over a short period of time because the power of the radio waves from the satellite attenuated and changes in cloud conditions affected the experiment. The results of the deformation measurement are shown in Fig. 16, and the measured displacements at the seven measurement points shown in Fig. 10 are summarized in Table 2. The coefficients of the Zernike modes were calculated from the measured deformation. The main reflector deformations under the applied weights of 44.1 N approximated by Zernike polynomials are shown in Fig. 17. The amplitudes of each Zernike mode are listed in Table 3. The results show that the most dominant Zernike mode is Z(2, 2), i.e., vertical astigmatism, as shown in Fig. 18. Some space antennas have position adjustment mechanisms for the sub-reflector [25] that can compensate the tip, tilt, and defocus errors. However, other deformation modes cannot be compensated by position adjustments. These deformations should be compensated by using the deformable reflector. In these experiments, the effects of Zernike modes Z(1, 1) and Z(1, −1) can be removed by the "five-point method." Therefore, the approximated deformation shapes using only the Z(2, 2) mode was used to obtain the optimum sub-reflector adjustment. The amplitude of the Z(2, 2) mode was 0.633 mm.

The actuator outputs were determined using the procedures explained in Section 2.3. The obtained actuator outputs are summarized in Table 4. The outputs of actuators nos. 3 and 6 were positive from the nominal state, and those of the other actuators were negative from the nominal state. These actuator outputs were consistent with the mode shape of the vertical astigmatism, which is the dominant mode of the deformation. However, these actuator outputs were the upper or lower stroke limits. This finding indicates that the path length errors due to the deformation of the main reflector were larger than the compensation ability of the deformable sub-reflector. The actuation of the deformable reflector is shown in Fig. 19. Fig. 20 shows the deformation of the sub-reflector obtained from the finite element analysis with actuator outputs shown in Table 4. The deformation was the difference of the deformed shape from the nominal shape. This figure indicates that the deformable reflector achieved a type of Z(2, 2) mode deformation. Comparing Figs. 18 and 20, the deformation shape was similar, but not identical because the surface shape of the deformable reflector had six petals to enlarge the achievable deformation.

The powers of the reception radio wave at each experimental step are summarized in Table 5. The reception power was decreased by 0.276 dB from the nominal state owing to the deformation of the main reflector. The deteriorated reception power was recovered by approximately 0.1 dB by adjusting the shape of the deformable reflector, and the results demonstrated the effectiveness of the path length error compensation by the developed smart reflector system.

However, the antenna reception power was not perfectly recovered mainly due to the limitation of the actuator strokes and the difference between the path length errors due to the deformation of the main reflector and the achievable path length changes by the deformable sub-reflector with six petals as shown in Fig. 20. The differences were caused by the fact that the main reflector used in this study was originally developed for a balloon-borne VLBI station, and the deformable sub-reflector was developed independently. To enhance the effectiveness of the deformable reflector system, it is important to match the deformation modes of the main reflector and the deformable sub-reflector which can be achieved using several strategies. One strategy is to use a deformable reflector having more actuators. We investigated it and its effectiveness was demonstrated through numerical simulations with the deformable reflector equipped with segmented mirrors and 12 actuators [26]. However, this strategy sometimes requires many actuators and amplifiers similar to earlier works [2-4], and consequently, the reflector system becomes complex. Another strategy is to design a main reflector and a deformable sub-reflector concurrently to match the deformation mode. This strategy can achieve high accuracy antenna optics by moderately complex sub-reflector system and the specially designed main reflector for the sub-reflector.

The half path length errors of the reflector system were calculated from geometrical optics analyses, and corresponding changes in antenna gains were analyzed using Physical Optics (PO) of GRASP software. The results are summarized in Table 6. Regarding antenna gains, the results were similar to the experimental results, and the difference was considered due to changes in cloud condition during the experiment. The half path length error of the reflector system was recovered from 0.44 mm RMS to 0.35 mm RMS by actuating the deformable reflector. This indicates both the effectiveness and limitation of this prototype. These path length errors were smaller than one-thirtieth of the wavelength used in this experiment (15 mm at 20 GHz) and the path length compensation was not necessary for this antenna. However, the path length compensation is necessary for higher frequency of radio waves, such as balloon-borne VLBI missions, and the changes in pathlength error of 0.1 mm RMS are more important. Therefore, the developed deformable antenna can improve antenna performance sufficiently for an antenna system using higher frequency radio waves.

The experiment could not be repeated due to changing weather. However, the repeatability of the deformations of the main reflector and the deformable sub-reflector were confirmed several times, and thus, same path length error compensations could be achieved using this antenna system.

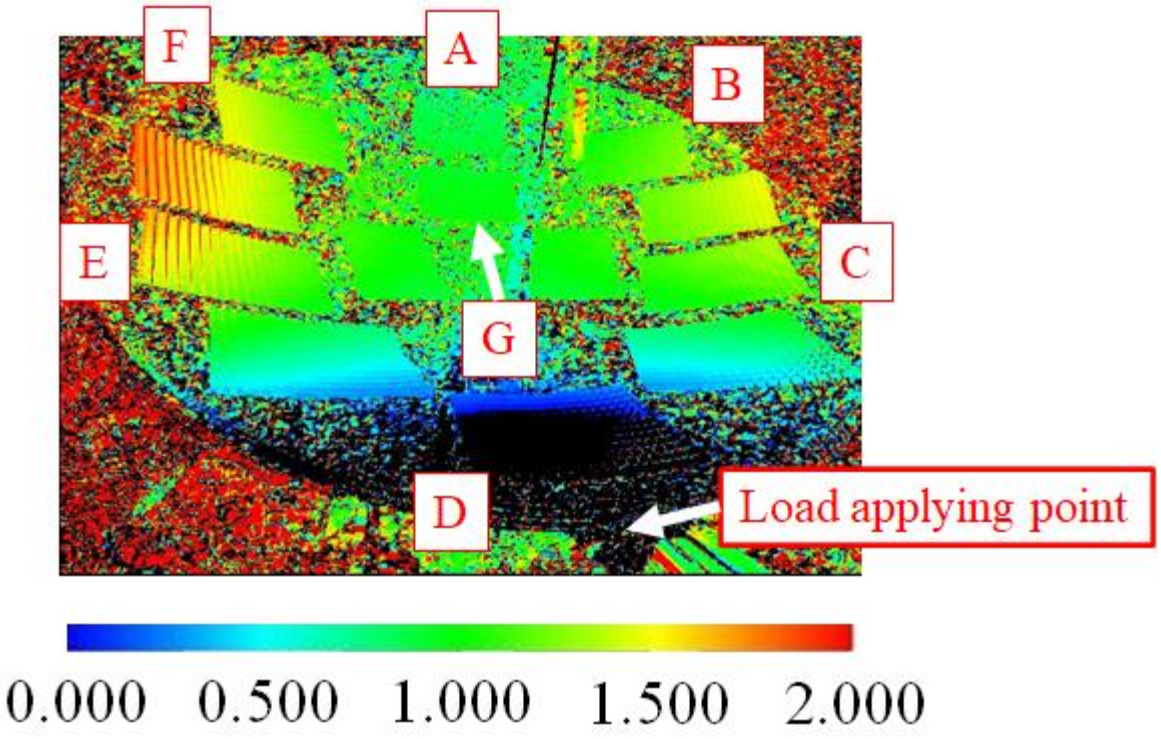

Fig. 16 Measured deformation of the main reflector [mm].

Table 2 Results of the deformation measurement

Measurement points	Displacement [mm]
A	0.958
B	1.134
C	1.157
D	−0.164
E	1.366
F	1.266
G	0.968

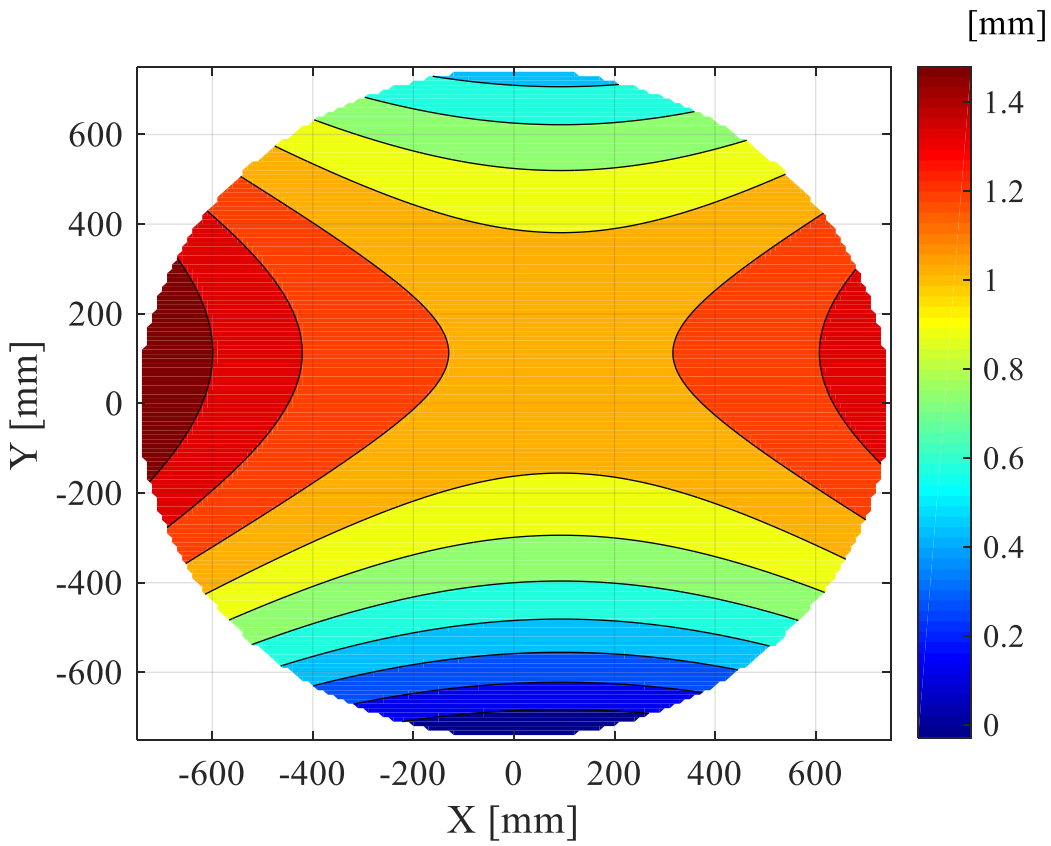

Fig. 17 Main reflector deformations approximated by Zernike polynomials.

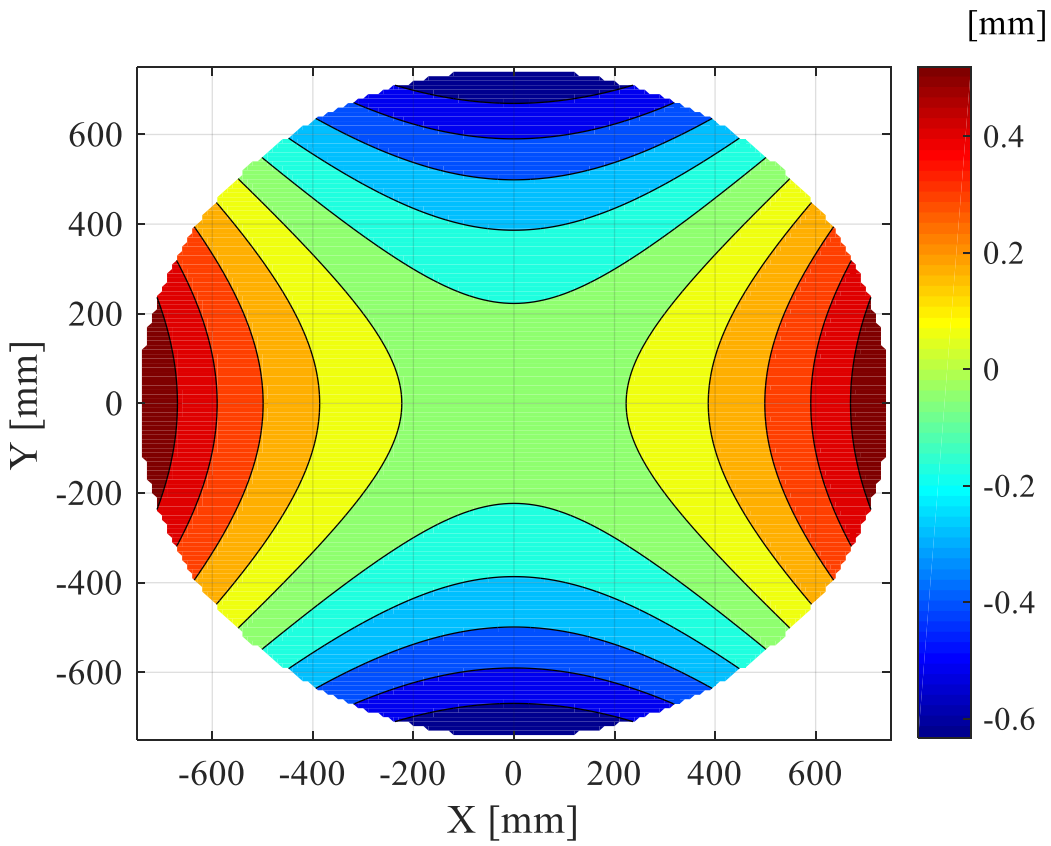

Fig. 18 Deformation shape of the dominant mode Z(2, 2).

Table 3 The amplitudes of each Zernike mode

Mode	Amplitude [mm]
Z(1, −1): Vertical tilt	0.269
Z(1, −1): Horizontal tilt	0.097
Z(2, 0): Defocus	0.128
Z(2, 2): Vertical astigmatism	0.633

Table 4 Actuator outputs for compensating the path length errors due to the load

No.	1	2	3	4	5	6
Output [mm]	0	0	1.0	0	0	1.0

*output of 0.5 mm is the nominal state of the actuators.

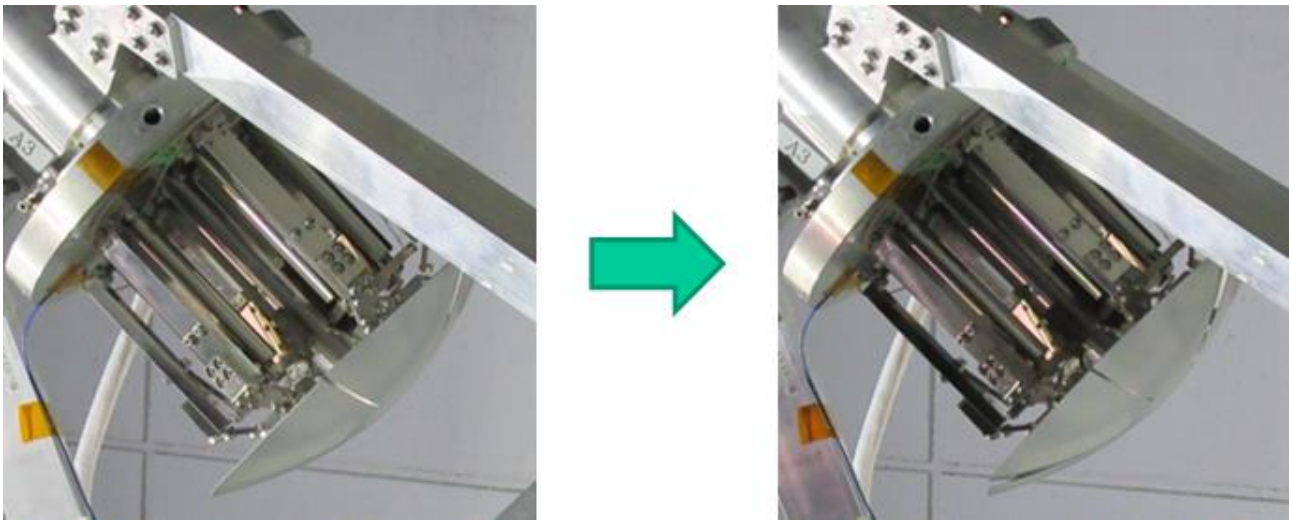

Fig. 19 Actuation of the deformable sub-reflector when the actuator output shown in Table 4 was applied.

(left: nominal state, right: deformable reflector was actuated)

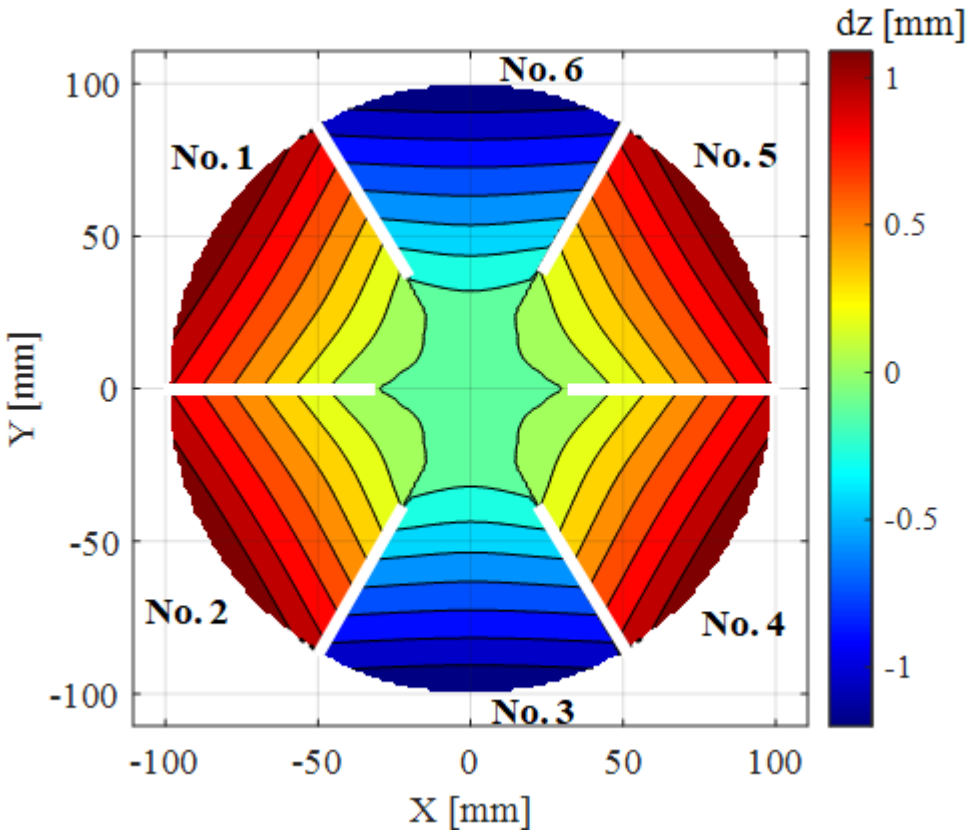

Fig. 20 Deformation of the deformable sub-reflector from the nominal state when the actuator output shown in Table 4 was applied. Z-direction is set to be the boresight direction and the deformations toward the horn antenna are shown in negative values.

Table 5 Powers of the received radio wave at each experimental step

Experimental steps	Power of the received radio wave [dB]	Changes in recaption power from the nominal state in experiments [dB]
Non-deformed main reflector without path length error compensation by the deformable reflector; nominal state.	−37.576	0
Deformed main reflector without path length error compensation by the deformable reflector.	−37.843	-0.276
Deformed main reflector with path length error compensation by the deformable reflector.	−37.742	-0.166

Table 6 The half path length error of the reflector system obtained by the geometrical optics analyses and changes in antenna gains analyzed using Grasp.

Experimental steps	Half path length error [mm RMS]	Changes in antenna gains [dB]
Non-deformed main reflector without path length error compensation by the deformable reflector; nominal state.	0	0
Deformed main reflector without path length error compensation by the deformable reflector.	0.44	-0.26
Deformed main reflector with path length error compensation by the deformable reflector.	0.35	-0.11

4. Conclusions

In this study, a high-precision reflector antenna system equipped with a deformable sub-reflector equipped with six actuators and a 2D grating measurement system was developed, and its effectiveness and limitation were experimentally demonstrated. In the system, a deformation of the main reflector of the antenna system was measured by a 2D grating measurement system, and the path length error owing to the deformation was compensated by adjusting the shape of the deformable sub-reflector. The novel path length error correction procedure for obtaining shape control inputs from shape measurement results at limited measurement points was also developed. In this method, the antenna deformations of the entire reflector area were estimated from the measured deformations at a small number of measurement points using Zernike polynomials, and this was used for obtaining the actuator outputs. The duration for measurement can be reduced by using this method, and this system can compensate the deformations

of the reflector, such as long-term deformations of an antenna structure and periodic thermal deformation. Incidentally, the response time of the deformable reflector is less than 1 second. Therefore, it can be used to quickly compensate the pathlength errors caused by vibration of a large antenna structure when an adequate vibration measurement system and a control method are employed.

In the experiment, the main reflector of the antenna system was deformed by applying a load, and the deformation was subsequently measured. The actuator outputs for compensating the path length error due to the deformation were obtained using the L-BFGS-B algorithm. Then, the actuation outputs were applied to the actuators, and the changes in the power of the radio waves received from the satellite were measured. The reception power was decreased by 0.267 dB from the nominal state owing to the deformation of the main reflector, and the deteriorated reception power was recovered by approximately 0.1 dB by adjusting the shape of the deformable reflector. This result demonstrates the effectiveness of the path length error compensation by the developed smart reflector system. However, the antenna reception power was not perfectly recovered, which was mainly due to the limitation of the actuator strokes and the difference between the path length errors by the deformation of the main reflector and the achievable path length changes by the deformable sub-reflector with six petals. Thus, it is important to match the deformation modes of the main reflector and the deformable sub-reflector to enhance the effectiveness of the deformable reflector system. The modified deformable reflector system will be employed in the balloon-borne VLBI mission.

Funding Sources

This study was supported by the Research Grant Program of the Institute of Space and Astronautical Science, Japan Aerospace Exploration Agency.

Acknowledgements

We would like to thank Editage (www.editage.com) for English language editing.

References

[1] Tanaka, H., Sakamoto, H., Inagaki, A., Ishimura, K., Doi, A., Kono, Y., Oyama, T., Watanabe, K., Oikawa, Y., and Kuratomi, T., "Development of a Smart Reconfigurable Reflector Prototype for an Extremely High-Frequency Antenna," *Journal of Intelligent Material Systems and Structures*, Vol. 27, 2016, pp. 764–773.
doi: 10.1177/1045389X15580660

[2] Fang, H., Quijano, U., Bach, V., Hill, J., and Wang, K.W., "Experimental Study of a Membrane Antenna Surface Adaptive Control System," 52nd AIAA/ASME/ASCE/AHS/ASC Structures, Structural Dynamics and Materials Conference; 19th AIAA/ASME/AHS Adaptive Structures Conference, 13t, Denver, Colorado, Apr. 4–7, 2011, AIAA-2011-1828.
doi: doi.org/10.2514/6.2011-1828

[3] Datashvili, L., Baier, H., Wei, B., Hoffman, J., Wehrle, E., Schreider, L., Mangenot, C., Prowald, J. S., Scolamiero, L., and Angevain, J.C., "Mechanical Investigations of in-Space-Reconfigurable Reflecting Surfaces," *32nd ESA Antenna Workshop on Antennas for Space Applications*, Noordwijk, The Netherlands, 2010, pp. 1–8.

[4] Bradford, S.C., Peterson, L.D., Ohara, C.M., Fang, S., Agnes, G.S., Hoffman, S.M., and Wilkie, W.K., "Piezocomposite Actuator Arrays for Correcting and Controlling Wavefront Error in Reflectors," 53rd AIAA/ASME/ASCE/AHS/ASC Structures, Structural Dynamics and Materials Conference, April 2012, AIAA 2012-1743.
doi: 10.2514/6.2012-1743.

[5] Wang, Z., Li, T., and Cao, Y., "Active Shape Adjustment of Cable Net Structures with PZT Actuators," *Aerospace Science and Technology*, Vol. 26, 2013, pp. 160–168.
doi: 10.1016/j.ast.2012.03.001

[6] Xie, Y., Shi, H., Alleyne, A., and Yang, B., "Feedback Shape Control for Deployable Mesh Reflectors Using Gain Scheduling Method," *Acta Astronautica*, Vol. 121, 2016, pp. 241–255.
doi: 10.1016/j.actaastro.2016.01.005

[7] JiaFu, L., Yu, F., Liang, Z., Na, L., Weiwei, W., Dan, Z., and ZhiGang, W., "Surface Shape Control of Integrated Paraboloid Space Reflector Consisting of Sub-Reflectors Exploiting Modulated Solar Pressure," *Advances in Space Research*, Vol. 67, 2021, pp. 1333–1349.
doi: 10.1016/j.asr.2020.11.017

[8] Molaei, A., Liu, C., Felton, S.M. and Martinez-Lorenzo, J., "Origami inspired reconfigurable antenna for wireless communication systems," arXiv preprint arXiv:1805.10370, 2018.

[9] Mihora, D.J., and Redmond, P.J., "Electrostatically Formed Antennas," *Journal of Spacecraft and Rockets*, Vol. 17, 1980, pp. 465–473.
doi: 10.2514/3.57766

[10] Zhang, Y., Gao, F., Zhang, S., and Hao, J., “Electrode Grouping Optimization of Electrostatic Forming Membrane Reflector Antennas,” *Aerospace Science and Technology*, Vol. 41, 2015, pp. 158–166.
doi: 10.1016/j.ast.2014.12.015

[11] Chao, L., and Yaoyao, S., “Comprehensive Structural Analysis and Optimization of the Electrostatic Forming Membrane Reflector Deployable Antenna,” *Aerospace Science and Technology*, Vol. 53, 2016, pp. 267–279.
doi: 10.1016/j.ast.2016.03.026

[12] Gu, Y., Duan, B., and Du, J., “The Establishment and Application of Direct Coupled Electrostatic-Structural Field Model in Electrostatically Controlled Deployable Membrane Antenna,” *Acta Astronautica*, Vol. 146, 2018, pp. 185–191.
doi: 10.1016/j.actaastro.2018.01.041

[13] H. Tanaka, H., Sakamoto, H., Inagaki, A., Ishimura, K., and Takahashi, K., “Development and evaluation of a smart reconfigurable reflector with slits,” 58th Space Sciences and Technology Conference, November 2014, 3B02. (in Japanese).

[14] Doi, A., Kono, Y., Kimura, K., Nakahara, S., Oyama, T., Okada, N., Satou, Y., Yamashita, K., Matsumoto, N., Baba, M., Yasuda, D., Suzuki, S., Hasegawa, Y., Honma, M., Tanaka, H., Ishimura, K., Murata, Y., Shimomukai, R., Tachi, T., Saito, K., Watanabe, N., Bando, N., Kameya, O., Yonekura, Y., Sekido, M., Inoue, Y., Sakamoto, H., Kogiso, N., Shoji, Y., Ogawa, H., Fujisawa, K., Narita, M., Shibai, H., Fuke, H., Uehara, K., and Koyama, S., “A Balloon-Borne Very Long Baseline Interferometry Experiment in the Stratosphere: Systems Design and Developments, “ *Advances in Space Research*, Vol. 63, 2019, pp. 779–793.
doi: 10.1016/j.asr.2018.09.020

[15] Wiktowy, M., O'Grady, M., Atkins, G., and Singhal, R., “Photogrammetric Distortion Measurements of Antennas in a Thermal-Vacuum Environment,” *25th ESA Antenna Workshop on Satellite Antenna Technology*, Noordwijk, The Netherlands, 2002, pp. 387–394.
doi: 10.5589/q03-008

[16] Ukita, N., Saito, M., Ezawa, H., Ikenoue, B., Ishizaki, H., Iwashita, H., Yamaguchi, N., and Hayakawa, T., “Design and Performance of the ALMA-J Prototype Antenna,” *Proceedings of the SPIE*, 5489, 2004, pp. 1085–1093.
doi: 10.1117/12.551523

[17] Talon, T., Chen, Y.L., and Pellegrino, S., “Shape Reconstruction of Planar Flexible Spacecraft Structures Using Distributed Sun Sensors,” *Acta Astronautica*, Vol. 180, 2021, pp. 328–339.
doi: 10.1016/j.actaastro.2020.12.056

[18] Torisaka, A., Hayashi, D., Kawasaki, S., Nishii, N., Terada, Y., Yokoyama, S., and Sakamoto, H., “Development of Shape Monitoring System Using SMA Dipole Antenna on a Deployable Membrane Structure,” *Acta Astronautica*, Vol. 160, 2019, pp. 147–154.

doi: 10.1016/j.actaastro.2019.04.007

[19] Iwasa, T., Tanaka, H., and Fujigaki, M., "Random Error Reduction Method for One-shot Shape Measurement Using the Grating Projection Method," *Transactions of the. Japan Society for Aeronautical and Space Sciences*, Vol. 58, 2015, pp. 337–344.

doi: 10.2322/tjsass.58.337

[20] Yamazaki, K., Higuchi, K., Katsumata, N., Iwasa, T., Kishimoto, N., and Fujigaki, M., "Deformation Measurement and the Analysis of Main Reflector for High Structural Accuracy Antenna System," *32nd International Symposium on Space Technology and Science*, 2019-c-42, Fukui, Japan, 2019, pp. 1–5.

[21] Li, T., Shi, J., and Tang, Y., "Influence of Surface Error on Electromagnetic Performance of Reflectors Based on Zernike Polynomials", *Acta Astronautica*, Vol. 145, 2019, pp. 396-407.

doi: 10.1016/j.actaastro.2018.01.063

[22] Lan, L., Jiang, S., Zhou, Y., Fang, H., Wu, Z., and Du, J., "Shape Control of a Reflector Based on Generalized Zernike Functions," AIAA Scitech, 3rd AIAA Spacecraft Structures Conference, January 2016, AIAA 2016-0704.

doi: 10.2514/6.2016-0704

[23] Byrd, R.H., Lu, P., Nocedal, J., and Zhu, C., "A Limited Memory Algorithm for Bound Constrained Optimization," *SIAM Journal on Scientific and Statistical Computing*, Vol. 16, No. 5, 1995, pp. 1190–1208.

doi: 10.1137/0916069

[24] Sakamoto, H., Tanaka, H., Ishimura, K., Doi, A., Kono, Y., Matsumoto, N., and Kimura, K., "Shape-Control Experiment of Space Reconfigurable Reflector Using Antenna Reception Power," 3rd AIAA Spacecraft Structures Conference. January 2016, AIAA 2016-0703.

doi: 10.2514/6.2016-0703

[25] Higuchi, K., Kishimoto, N., Meguro, A., Tanaka, H., Yoshihara, M., and Iikura, S., "Structure of High Precision Large Deployable Reflector for Space VLBI (Very Long Baseline Interferometry)," 50th AIAA/ASME/ASCE/AHS/ASC Structures, Structural Dynamics, and Materials Conference, May 2009, AIAA 2009-2609.

doi: 10.2514/6.2009-2609

[26] Sakano, F., Kogiso, N., Tanaka, H., and Iwasa, T., Multiobjective Optimal Actuator Layout for Smart Antenna System Considering Operational Uncertainties, *Journal of the Japan Society for Aeronautical and Space Science*, Vol.69, No.4, 2021, pp. 169-179. (in Japanese) doi: 10.2322/jjsass.69.169